Title

Preferential Lymphatic Growth in Bronchus-Associated Lymphoid Tissue in Sustained Lung Inflammation

Journal

American Journal Of Pathology, 184(5)

ISSN

0002-9440

Authors

Baluk, Peter
Adams, Alicia
Phillips, Keeley
et al.

Publication Date

2014-05-01

DOI

10.1016/j.ajpath.2014.01.021

Peer reviewed

The American Journal of Pathology, Vol. 184, No. 5, May 2014

The American Journal of
PATHOLOGY
ajp.amjpathol.org

VASCULAR BIOLOGY, ATHEROSCLEROSIS, AND ENDOTHELIUM BIOLOGY

Preferential Lymphatic Growth in Bronchus-Associated Lymphoid Tissue in Sustained Lung Inflammation

Peter Baluk,* Alicia Adams,* Keeley Phillips,* Jennifer Feng,* Young-Kwon Hong,† Mary B. Brown,‡ and Donald M. McDonald*

From the Department of Anatomy, the Cardiovascular Research Institute, and the Comprehensive Cancer Center, University of California, San Francisco, California; the Departments of Surgery, Biochemistry, and Molecular Biology,† Norris Comprehensive Cancer Center, Keck School of Medicine, University of Southern California, Los Angeles, California; and the Department of Infectious Diseases and Pathology,‡ College of Veterinary Medicine, University of Florida, Gainesville, Florida*

Accepted for publication January 7, 2014.

Address correspondence to Peter Baluk, Ph.D., University of California, 513 Parnassus Ave, San Francisco, CA 94143-0452. E-mail: peter.baluk@ucsf.edu.

Lymphatics proliferate, become enlarged, or regress in multiple inflammatory lung diseases in humans. Lymphatic growth and remodeling is known to occur in the mouse trachea in sustained inflammation, but whether intrapulmonary lymphatics exhibit similar plasticity is unknown. We examined the time course, distribution, and dependence on vascular endothelial growth factor receptor (VEGFR)-2/VEGFR-3 signaling of lung lymphatics in sustained inflammation. Lymphatics in mouse lungs were examined under baseline conditions and 3 to 28 days after *Mycoplasma pulmonis* infection, using prospero heomeobox 1–enhanced green fluorescence protein and VEGFR-3 as markers. Sprouting lymphangiogenesis was evident at 7 days. Lymphatic growth was restricted to regions of bronchus-associated lymphoid tissue (BALT), where VEGF-C–producing cells were scattered in T-cell zones. Expansion of lung lymphatics after infection was reduced 68% by blocking VEGFR-2, 83% by blocking VEGFR-3, and 99% by blocking both receptors. Inhibition of VEGFR-2/VEGFR-3 did not prevent the formation of BALT. Treatment of established infection with oxytetracycline caused BALT, but not the lymphatics, to regress. We conclude that robust lymphangiogenesis occurs in mouse lungs after *M. pulmonis* infection through a mechanism involving signaling of both VEGFR-2 and VEGFR-3. Expansion of the lymphatic network is restricted to regions of BALT, but lymphatics do not regress when BALT regresses after antibiotic treatment. The lung lymphatic network can thus expand in sustained inflammation, but the expansion is not as reversible as the accompanying inflammation. *(Am J Pathol 2014, 184: 1577–1592; http://dx.doi.org/10.1016/j.ajpath.2014.01.021)*

Lymphatic vessels undergo changes in many inflammatory lung diseases, where lymphatic proliferation, enlargement, and regression have been described.[1,2] Examples include asthma, where lymphatics regress,[3] chronic obstructive pulmonary disease (COPD) and pneumonia, where they proliferate,[4–6] and idiopathic pulmonary fibrosis, where they undergo abnormal growth and remodeling in the lung parenchyma[7,8] but regress in subpleural and interlobular compartments.[9]

Although lymphatics are well known to drain interstitial fluid and serve as conduits for antigen-presenting cells and lymphocytes from the lung,[10–12] little has been learned about the mechanism and functional implications of lymphatic changes in pulmonary inflammation. Regardless of the impact of lymphangiogenesis on disease pathophysiological characteristics, the presence of edema in inflammatory lung disease indicates that the amount of plasma leakage exceeds the fluid drainage capacity through lymphatics and other routes.

Lymphatics proliferate in many settings of sustained inflammation, including psoriasis,[13] rheumatoid arthritis,[14] and inflammatory bowel disease,[15] but it is still unclear whether proliferation of lymphatics worsens or ameliorates disease severity. Promotion of lymphatic growth by transgenic overexpression of vascular endothelial growth factor (VEGF)-C reduces the severity of skin inflammation.[16] This effect has not been examined in the lung, and

This work was supported in part by funding from grants HL024136 and HL59157 from National Heart, Lung, and Blood Institute of the U.S. National Institutes of Health, AngelWorks, and from the Leducq Foundation (D.M.M.).

Disclosures: None declared.

http://dx.doi.org/10.1016/j.ajpath.2014.01.021

it is unknown whether it is typical of inflammatory conditions in other organs. It is also unclear whether lung lymphatics exhibit the same plasticity in inflammation as those in other organs.

Previous studies had shown that tracheal lymphatics undergo widespread growth and remodeling after infection. During the first 4 weeks after infection, tracheal lymphatics undergo even more extensive changes than blood vessels.[17,18] However, sensitization and challenge of lungs to house dust mite allergen for 2 weeks has no detectable effect on the number of lung lymphatics.[19] Little is known about the effects on lung lymphatics of other conditions of sustained inflammation.

We, therefore, used a mouse model of sustained lung inflammation produced by respiratory tract infection by *Mycoplasma pulmonis* bacteria to determine the response of lung lymphatics to sustained inflammation and to compare changes in the lung with those in the trachea. With the presumption that lymphangiogenesis does occur in the lung, we sought to determine exactly when and where. During the period of 1 to 4 weeks after infection, we closely observed the distribution of the changes in the lung to address the possibility that lymphatic growth or remodeling was regionally specific.

We also investigated the driving mechanism for lymphatic growth in lungs in this model. Because of compelling evidence that lymphatic growth in the trachea and other settings is driven by VEGF-C activation of VEGF receptor (VEGFR)-3 signaling,[20] we compared the effects in the lung and trachea of blocking VEGFR-2 and VEGFR-3 administered individually or together.

Consistent with this reasoning, previous studies revealed that lymphangiogenesis in the trachea after *M. pulmonis* infection was completely inhibited by a function-blocking antibody to VEGFR-3.[17] Similar results have been obtained in skin[21] and cornea.[22] However, lymphangiogenesis under some conditions is also partially reduced by selective inhibition of VEGFR-2, examples being skin,[23] cornea,[24] lymph nodes,[25] arthritic joints,[24] and tumors.[26] The latter mechanism could reflect effects of VEGFR-2 blockade directly on lymphatics or indirectly through changes in leukocytes or other cells that produce lymphangiogenic factors.

The present study of lymphatic remodeling in sustained bronchopneumonia produced by *M. pulmonis* infection addressed the question of whether lymphatics grow, undergo remodeling, or regress during the development of bronchopneumonia. The study also examined the time course of changes in lymphatics, whether the distribution of lymphangiogenesis coincides with the widespread inflammatory changes in the lung, and whether lymphatic growth and remodeling in the lung is driven by changes in signaling of VEGFR-3, VEGFR-2, or both.

The experiments revealed that some lymphatics in the lung underwent profound changes after *M. pulmonis* infection. Sprouting lymphangiogenesis was evident at 1 week and was more pronounced at 2 and 4 weeks. Strikingly, expansion of the lymphatic network was restricted to regions of bronchus-associated lymphoid tissue (BALT) that formed in the lung around bronchi and major pulmonary vessels. Lymphatics in more peripheral regions of the lung did not exhibit these changes, despite the presence of inflammatory cells. Growth of lymphatics in BALT was blocked 99% by inhibition of VEGFR-2 and VEGFR-3 together. Inhibition of VEGFR-3 alone resulted in 83% reduction, whereas inhibition of VEGFR-2 alone resulted in 68% reduction. Inhibition of lymphangiogenesis in BALT by blocking VEGFR-2 and VEGFR-3 did not prevent the formation of BALT.

Materials and Methods

Mice

Mice used were C57BL/6 strain, specific pathogen free, and housed under barrier conditions. They included wild-type mice (Charles River, Hollister, CA), prospero heomeobox 1 (Prox1)−enhanced green fluorescence protein (EGFP)−transgenic mice with fluorescent green lymphatics,[27] and CC10−VEGF-A−transgenic mice overexpressing human VEGF-A in epithelial cells of airways and lungs.[28] Mice were anesthetized by i.m. injection of 87 mg/kg ketamine and 13 mg/kg xylazine. The Institutional Animal Care and Use Committee of the University of California, San Francisco, approved all experimental procedures.

M. pulmonis Infection and Antibiotic Treatment

Anesthetized mice were infected with *M. pulmonis* by intranasal inoculation of 25 μL per nostril of broth containing a total of 10^6 colony-forming units of organisms (strain CT7), as described previously.[17] In some experiments, mice were treated for 14 days by daily i.p. injection of 100 mg/kg oxytetracycline (Liquamycin; Pfizer, Sao Paulo, Brazil) to eliminate the infection.

Inhibition of VEGF-2 and/or VEGFR-3 Signaling

Function-blocking rat monoclonal antibodies were used to block VEGFR-2 (clone DC101) and/or VEGFR-3 (clone mF4-31C1) (ImClone Systems, New York, NY).[17] Antibodies were injected i.p. at a dose of 0.8 mg in a volume of 200 μL of 0.9% sterile NaCl solution per mouse 1 day before infection, then every other day for 14 days. Rat IgG (Jackson ImmunoResearch Labs Inc., West Grove, PA) was used as a control.

Fixation and Tissue Preparation

The vasculature of anesthetized mice was perfused for 2 minutes at a pressure of 120 to 140 mmHg with fixative (1% paraformaldehyde in PBS, pH 7.4; Sigma-Aldrich, St. Louis, MO) from a cannula inserted through the left

ventricle into the aorta. In some cases, the pulmonary circulation was first flushed by insertion of the cannula into the right ventricle at the origin of the pulmonary artery and perfusion at a pressure of 20 mmHg until the lungs turned white. To preserve alveoli in an expanded condition, lungs were inflated with 0.4 mL of melted 1% SeaPlaque low-melting point agarose (Lonza, Rockland, ME) in PBS slowly administered intratracheally via a syringe and an 18-gauge catheter. Tracheas, bronchial lymph nodes, and lungs were removed, weighed, and immersed in fixative for 1 hour at 4°C and then washed with PBS. The left lung was cut transversely into three parts, such that the middle part contained the main bronchus and the major pulmonary blood vessels were cut in cross section approximately 3 mm below the hilum (Figure 1). The left lung sections and whole right lungs were embedded flat in Tissue-Tek medium (Sakura, Torrance, CA) and frozen as cryostat blocks.

IHC Data

Tissues were washed and stained immunohistochemically (IHC) by incubating cryostat sections (200 μm thick) of the mid left lung cut transversely or whole mounts of trachea with one or more primary antibodies diluted in PBS containing 0.3% Triton X-100 (Sigma-Aldrich), 0.2% bovine serum albumin (Sigma-Aldrich), 10% normal serum (Jackson ImmunoResearch Labs Inc.), and 0.1% sodium azide (Sigma-Aldrich).[17] We used the following antibodies to identify blood vessels: platelet endothelial cell adhesion molecule (PECAM)-1 (CD31) (hamster anti-mouse monoclonal, clone 2H8, MA3105; Thermo Fisher Scientific, Rockford, IL); lymphatics, such as VEGFR-3 (goat anti-mouse polyclonal AF743; R&D Systems, Minneapolis, MN); lymphatic vessel endothelial cell marker (LYVE)-1 (rabbit anti-mouse polyclonal 11-034; AngioBio, Del Mar, CA); podoplanin (Syrian hamster anti-mouse monoclonal, clone 8.1.1; AngioBio); neuropilin-2 (goat polyclonal AF567; R&D Systems); chemokine ligand (CCL) 21 (goat polyclonal AF457; R&D Systems); VEGF-C (goat polyclonal sc-7132; Santa Cruz Biotechnology, Dallas, TX); Prox1 (rabbit anti-mouse polyclonal AB5475; Millipore, Billerica, MA); smooth muscle cells, such as α-smooth muscle actin (αSMA; mouse monoclonal, clone 1A4 conjugated to fluorescein isothiocyanate, F3777, or Cy3; C6198; Sigma-Aldrich); pan-leukocyte marker CD45 (rat anti-mouse monoclonal, clone 30-F11; BioLegend, San Diego, CA); B lymphocytes, such as B220 (rat anti-mouse monoclonal, clone RA3-6B2; BD Biosciences, San Jose CA); T lymphocytes, such as CD3e (Armenian hamster anti-mouse monoclonal, clone 145-2C11; BD Biosciences); macrophages and dendritic cells, such as allograft inflammatory factor 1/ionized calcium-binding protein 1 (Aif1/Iba1; Wako USA, Richmond, VA); neutrophils, such as S100A8 (goat polyclonal AF3059; R&D Systems); high endothelial venules (HEVs), such as MECA-79 (PNAd carbohydrate epitope, CD62L, rat anti-mouse monoclonal, clone MECA-79; BD Biosciences); lung epithelial cells (primarily alveolar type 1 cells), such as aquaporin-5 (rabbit polyclonal ab78486; Abcam, Cambridge, MA) or pan-cytokeratin (rabbit polyclonal Z0622; Dako USA, Carpinteria, CA); epithelial microfold cells (M cells), such as biotinylated *Ulex europaeus* lectin B1065 (Vector Laboratories, Burlingame, CA); and endogenous EGFP fluorescence, amplified by chicken polyclonal anti-GFP (GFP-1020; Aves Labs, Tigard, OR).

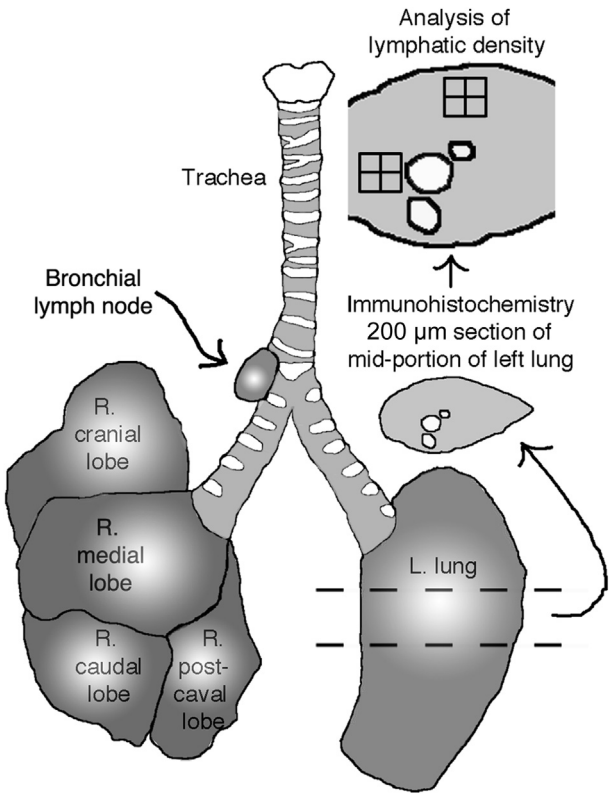

Figure 1 Schematic of mouse lungs and regions used for analysis. The midportion of the left (L.) lung was embedded flat, and cryostat sections (200 μm thick) were stained IHC and then analyzed to compute the abundance of lymphatics by superimposing stereological counting grids on projected microscope images of lung regions of standard size. Lungs and bronchial lymph nodes were weighed. L, left; R, right.

Secondary antibodies were labeled with Dy488 or Alexa488, Cy3, or Cy5 or Dy649 (Jackson ImmunoResearch Labs Inc.). Specimens were viewed with a Zeiss Axiophot fluorescence microscope (Zeiss USA, Thornwood, NY) equipped with a three−charge-coupled device low-light red, green, blue (RGB) video camera (CoolCam; SciMeasure, Decatur, GA) or a Zeiss LSM-510 confocal microscope using AIM 4.0 confocal software version 4.0 (Zeiss USA).

Preliminary experiments showed that the most effective markers for lymphatics in mouse lungs were EGFP in Prox1-EGFP−transgenic mice and VEGFR-3. The IHC amplified Prox1-EGFP provided strong staining of lymphatics with little or no background staining. Other conventional markers, including LYVE-1 and podoplanin (gp38, T1α), were not as useful for identifying lymphatics in mouse lung because of expression in other cell types (Supplemental Figure S1, A and B). Pulmonary blood vessels and tissue macrophages had strong LYVE-1 immunoreactivity. Type 1 alveolar epithelial

cells had strong podoplanin immunoreactivity. Immunoreactivity for neuropilin-2, a coreceptor for VEGFR-3, was stronger in smaller- than in larger-diameter lymphatics (Supplemental Figure S1C).

Measurement of Lymphatics and BALT

The area density of lymphatics was measured in transverse sections (200 μm thick) of the middle portion of the left lung. The left lung, consisting of only one lobe, was used for measurements because of its simpler structure compared with the multiple-lobed right lung. To identify the main stem bronchus, pulmonary artery, and pulmonary vein and provide a reference framework for the lymphatics, we stained smooth muscle cells in the walls of airways and blood vessels for αSMA.[19] For morphometry, lung slices were stained for VEGFR-3 instead of Prox1-EGFP, which was also expressed in cardiac muscle cells of the proximal portion of the pulmonary vein and tended to obscure the surrounding lymphatic vessels. Sections of the midportion of the left lung were imaged with 10× (numerical aperture, 0.5) objective lenses linked to a video camera and digitizing tablet, and images were projected onto a color monitor, as described previously.[17] A rectangular survey box with an area of 0.134 mm^2 consisting of 126 points arranged in a simple square grid was superimposed on the projected image of each of four regions: the main stem bronchus, pulmonary vein, pulmonary artery, and lung parenchyma. The survey box was positioned with one edge located along the transversely cut edge of the bronchus, pulmonary artery, or pulmonary vein, as identified by staining for αSMA so that the box contained lymphatics associated only with that particular structure (Figure 1). For the lung parenchyma, the survey box was positioned over regions of the peripheral lung that had minimal αSMA immunoreactivity. The number of survey grid points overlying tubular structures corresponding to lymphatics was counted and expressed as a percentage of the total. Lungs from at least five mice per group were counted for each condition. For comparison, lymphatic area densities were also determined in whole mounts of tracheas stained for LYVE-1 immunoreactivity, with the survey box positioned over the regions of mucosa overlying the cartilage rings.[17] The diameter of lymphatics was measured in sections stained for VEGFR-3 or Prox1-EGFP. BALT was quantified by measuring the area of regions of densely packed lymphoid cells in H&E-stained sections of the midportion of the left lung with the digitizing tablet at a magnification of ×75 and was expressed as a percentage of total lung area.

Statistical Analysis

Values are presented as means ± SEM, with at least five mice per group unless otherwise indicated. The significance of differences between groups was assessed by analysis of variance, followed by the Dunn-Bonferroni test for multiple comparisons, with $P < 0.05$ considered significant.

Results

Distribution of Lymphatics in Normal Lung

The effect of *M. pulmonis* infection on lung lymphatics was determined by first obtaining baseline data for the distribution of lymphatics in the lungs of pathogen-free mice. The approach was to visualize lymphatics by immunofluorescence staining for Prox1-EGFP or VEGFR-3 in thick slices of the midportion of the left lung of mice (Figure 1). Smooth muscle cells of airways and blood vessels in the slices were similarly stained for αSMA to serve as reference structures.

Most lymphatics in lungs of pathogen-free mice were located around large bronchi and major blood vessels near the hilum (Figure 2A). Bronchi, pulmonary arteries, and pulmonary veins could be distinguished from one another by their characteristic arrangement of smooth muscle cells. A common network of lymphatics surrounded pairs of bronchi and pulmonary artery branches (Figure 2, A and B). A seemingly separate lymphatic network surrounded pulmonary veins (Figure 2, C–E). Lymphatics accompanied airways and blood vessels into the lung parenchyma. The lymphatic network extended further distally along the branches of pulmonary veins than pulmonary arteries or airways of comparable diameter (Figure 2C).

The number and distribution of lymphatics around bronchi, pulmonary artery, pulmonary vein, and distal regions of the lung under pathogen-free conditions provided a reference for understanding changes that occurred after infection. Near the lung hilum, lymphatics were comparably numerous around the main stem bronchus, pulmonary artery, and pulmonary vein (Figure 2F). However, lymphatics were <20% as abundant in alveolar regions containing only small airways or blood vessels of the distal lung parenchyma. In pathogen-free lungs, the mean diameter of the largest lymphatics was 60 ± 7 μm at their entry at the hilum and 38 ± 7 μm on medium-sized airways and vessels. The smallest lymphatics detected on terminal branches of pulmonary veins (Figure 2, C–E) had a diameter of 9 ± 1 μm. Even near alveoli and visceral pleura, lymphatics were typically associated with airways and blood vessels (Figure 2, C–E). Few lymphatics were located within or beneath the visceral pleura (Figure 2, A, C, and E).

Expansion of Lung Lymphatic Network after *M. pulmonis* Infection

Lymphatics were conspicuously more abundant in lungs of infected mice than in lungs of pathogen-free mice (Figures 2A and 3A, respectively). Evaluation of lung sections at 0, 7, 14, and 28 days after *M. pulmonis* infection revealed that the lymphatic network expanded progressively during this period. Most of the lymphangiogenesis occurred around major bronchi, pulmonary arteries, and pulmonary veins (Figure 3, A–C). From 7 days of infection onward, lymphatics around bronchi and pulmonary vessels had abundant endothelial sprouts; by comparison, lymphatics in pathogen-free lungs

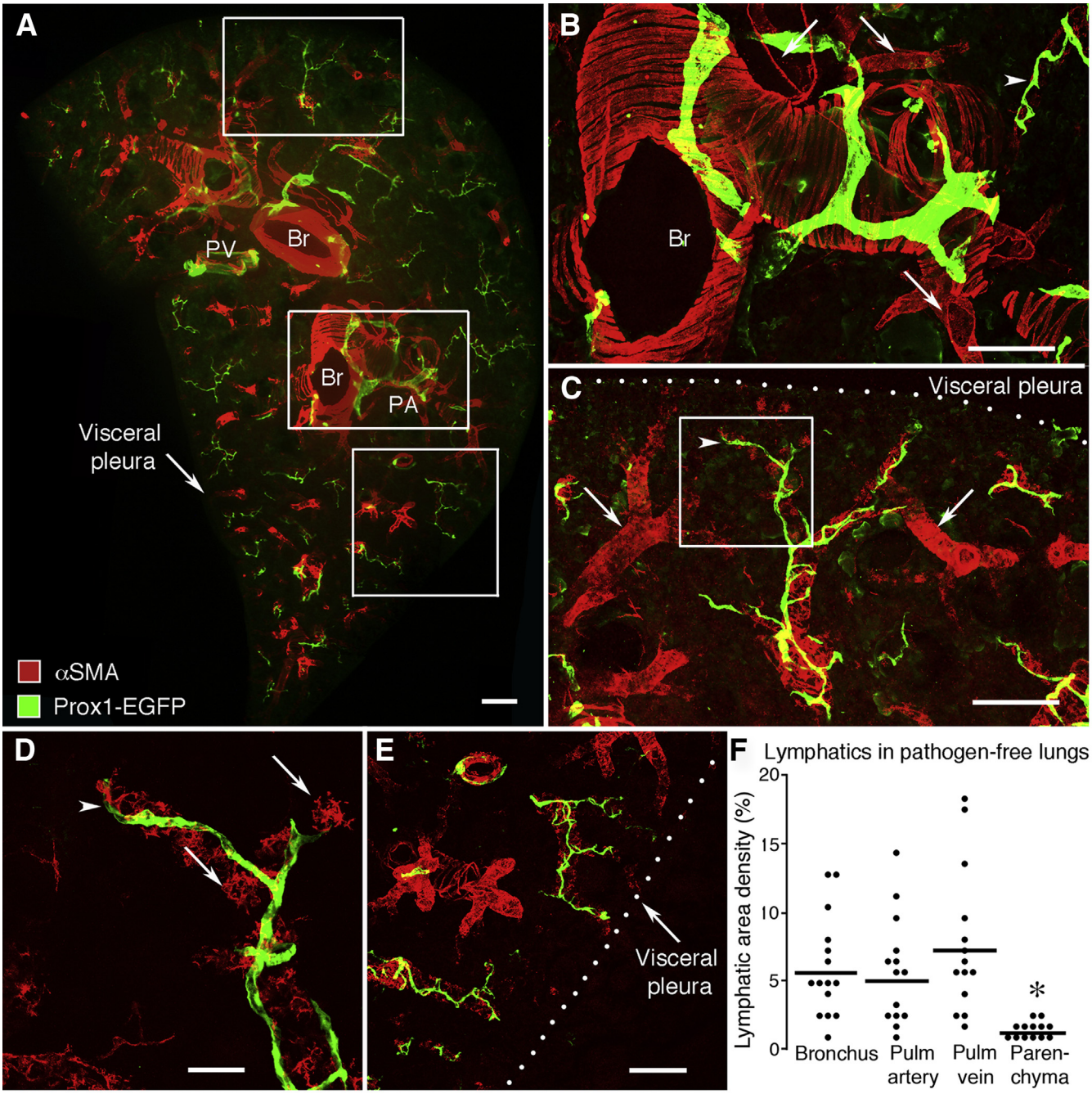

Figure 2 Number and distribution of lymphatics in lung of pathogen-free mice. Lymphatics are stained for Prox1-EGFP immunoreactivity (green). Smooth muscle cells stained for αSMA (red) delineate the wall of airways and blood vessels. **A:** Overview of the distribution of lymphatics in the midportion of the left lung. Lymphatics encircle major bronchi and blood vessels and follow branches toward the lung perimeter. No lymphatics are present in the visceral pleura. **Boxed** regions in **A** are shown enlarged in **B** (**A**, **middle box**), **C** (**A**, **top box**), and **E** (**A**, **bottom box**) **B:** Smooth surfaced lymphatics on bronchus (Br) near the hilum. Typical of bronchi, bands of smooth muscle cells (αSMA, red) are oriented perpendicular to the airway axis. Also visible are small branches of the pulmonary artery (PA; **arrows**) and pulmonary vein (PV; **arrowhead**). **C:** Smooth surfaced lymphatics on a small branch of PV (**arrowhead**). Small branches of PA that lack lymphatics are also visible (**arrows**). **D:** Enlargement of **boxed** region in **C** showing the relationship of lymphatics (**arrowhead**) to smooth muscle of small PV (**arrows**). **E:** Lymphatics in distal lung on small branches of PV. **F:** Relative abundance of lymphatics around major bronchi, branches of PA and vein, and distal lung parenchyma in cross section (200 μm thick) of the mid region of the left lung. Dots show the mean area density of lymphatics marked by VEGFR-3 staining in each mouse. Values for Br and pulmonary vessels are not significantly different from one another. $^*P < 0.05$ between Br and pulmonary vessels ($N = 13$ to 15 mice per group). Scale bars: 200 μm (**A**–**C** and **E**); 50 μm (**D**).

had a smooth surface (Figure 3, D and E). Regions around large bronchi and pulmonary vessels, where lymphatics were most abundant, were sharply demarcated from regions of type 1 alveolar epithelial cells in lung alveoli (Figure 3, F and G).

The increase in lymphatics was approximately equivalent around large bronchi, pulmonary arteries, and pulmonary veins. Overall values calculated from average values for the three regions were used to determine the time course of

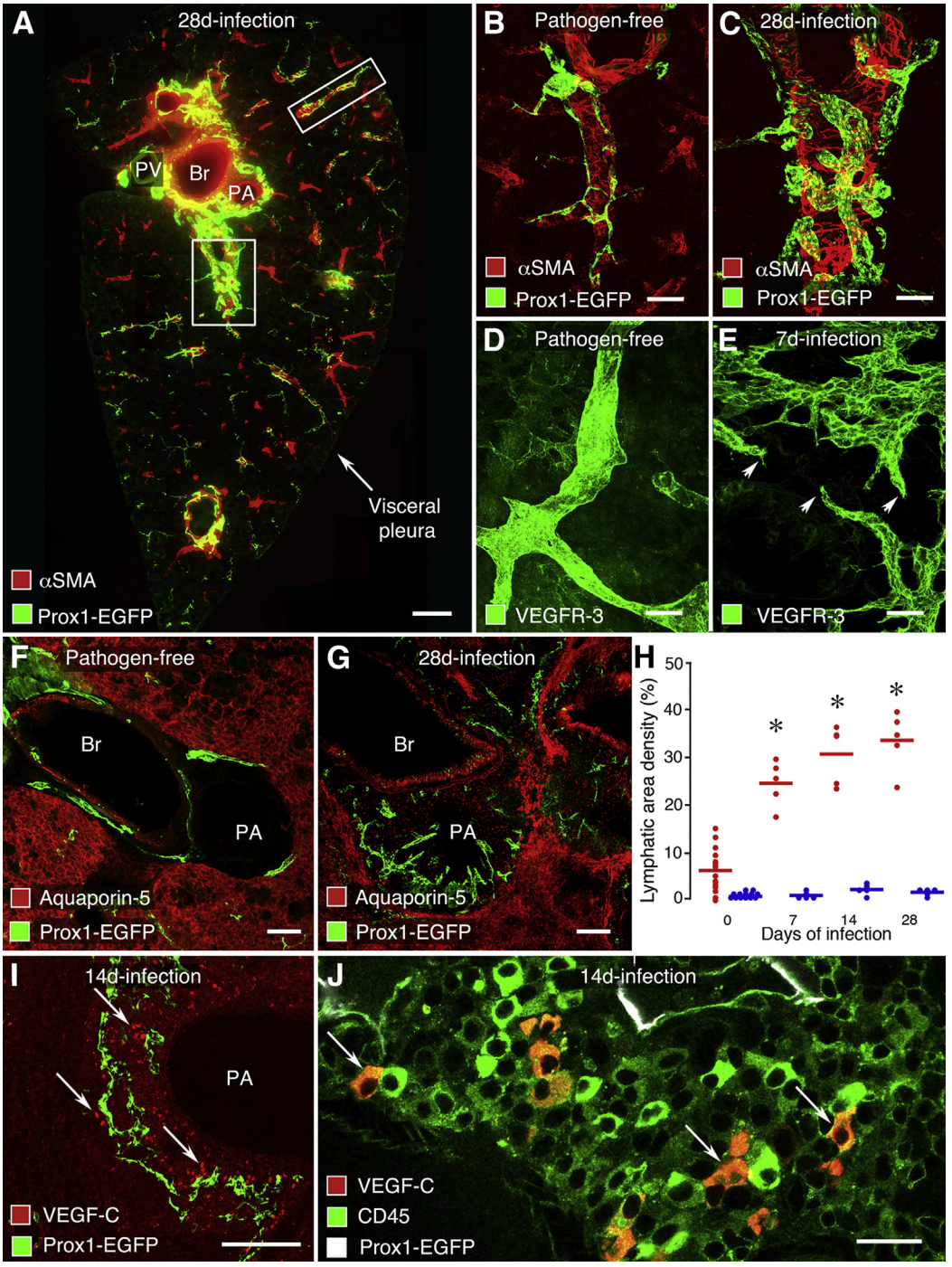

Figure 3 Expansion of lymphatic network in mouse lung after *M. pulmonis* infection. **A:** Overview of lymphatics in the midportion of the left lung near the hilum after infection for 28 days. Abundant lymphatics (Prox1-EGFP, green) found around major bronchus (Br), pulmonary artery (PA), and pulmonary vein (PV), shown by smooth muscle (αSMA, red) in the wall, but few lymphatics in the distal lung. **Boxed** regions are shown enlarged in **C** (**A**, **lower box**) and Supplemental Figure S2A (**A**, **upper box**). Comparison of few small lymphatics (Prox1-EGFP, green) on a pulmonary vein branch in lung of pathogen-free mouse (**B**) with abundant larger lymphatics on a pulmonary vein after infection for 28 days (**C**). Comparison of smooth surfaced lymphatic in lung of pathogen-free mouse (**D**) and lymphatics with sprouts (**arrowheads**) in lung after infection for 7 days (**E**). Lymphatics shown by VEGFR-3 immunoreactivity (green). Comparison of few lymphatics (Prox1-EGFP, green) in the narrow space around Br and PA of lung of pathogen-free mouse (**F**) with abundant lymphatics in cuff of lymphoid tissue around pulmonary artery and bronchus after infection for 28 days (**G**). Region of lymphatics in lymphoid tissue is sharply demarcated from surrounding lung parenchyma with type 1 alveolar epithelial cells shown by aquaporin-5 immunoreactivity (red). **H:** Time course of expansion of lymphatic network in left lung from pathogen-free state (0) to 7, 14, and 28 days after infection. Each red dot represents the average value for lymphatics near bronchi, pulmonary arteries, and pulmonary veins in each mouse at one time point. Mean values after infection are significantly different from baseline ($^*P < 0.05$). Blue dots are corresponding values for lung parenchyma, which are significantly less than red values but not different from one another ($N = 4$ to 15 mice per group). **I:** Cells with VEGF-C immunoreactivity (red, **arrows**) near lymphatics (Prox1-EGFP, green) in BALT around PA after infection for 7 days. **J:** Higher-magnification view of **I** showing the distribution of cells in which staining for VEGF-C (red) and CD45 (green) are colocalized (orange, **arrows**). Scale bars: 200 μm (**A**, **F**, and **G**); 50 μm (**B**–**E** and **I**); 20 μm (**J**). Br, bronchi; PA, pulmonary artery.

lymphatic network expansion (Figure 3H). These data revealed that the lymphatic network expanded threefold during the first 7 days after infection and continued to increase to approximately sixfold at 28 days (Figure 3H). In sharp contrast to these regions, lymphatics in the lung parenchyma did not increase after infection (Figure 3H). Few sprouts were found on lymphatics on distal regions of lung parenchyma, including small bronchi, blood vessels (Supplemental Figure S2A), and visceral pleura.

Further changes in lung lymphatics after infection included stronger CCL21 immunoreactivity in lymphatic endothelial cells (Supplemental Figure S2, B–G). CCL21 was widespread in lung lymphatics after infection, was relatively specific to lymphatic endothelial cells, and contrasted with weak staining in pathogen-free lungs, where it was restricted to the perinuclear region of lymphatic endothelial cells (Supplemental Figure S2, B–G). No change was detected in the intensity of VEGFR-3 or Prox1-EGFP immunoreactivity in lymphatics after infection. LYVE-1 and podoplanin antibodies proved to be unsuitable for staining lymphatics in the lung because they also labeled other cell types. Immunoreactivity for neuropilin-2, a coreceptor for VEGFR-3, was not uniformly strong on lymphatics of all sizes to be used as a reliable marker (Supplemental Figure S1, A–C).

In search of potential drivers of lymphatic growth and remodeling after infection, we examined the distribution and abundance of cells that express the potent lymphangiogenic factor, VEGF-C. We found that VEGF-C–immunoreactive cells were located preferentially in BALT around large bronchi and pulmonary vessels (Figure 3, I and J). VEGF-C–positive cells were numerous in regions of the expanded lymphatic network in BALT, but were sparse or absent in the adjacent lung parenchyma (Figure 3I). Staining for CD45 identified the VEGF-C–immunoreactive cells as a subpopulation of mononuclear leukocytes (Figure 3J).

Preferential Growth of Lymphatics in BALT after *M. pulmonis* Infection

Distribution of Inflammation after Infection

The progression of lung inflammation after *M. pulmonis* infection was examined in H&E-stained sections at 0, 7, 14, and 28 days after infection. Two concurrent processes were evident: formation of cuffs of lymphoid tissue around inflamed airways and major blood vessels and accumulations of inflammatory cells in alveoli typical of lobar pneumonia (Figure 4A). Peribronchial and perivascular accumulations of lymphoid tissue fit with published descriptions of BALT.[29–33] Cell infiltration increased with duration of infection, and at 28 days, some regions of lung parenchyma were consolidated by inflammatory cell infiltrate (Figure 4, A and B).

The amount of BALT increased from none in pathogen-free lungs to an average of >15% of the total lung area at 28 days of infection, but it varied among mice at each time point and at 28 days ranged from almost none to 30% (Figure 4C). The mean wet weight of the left lung increased 2.5-fold during this period (Figure 4D). Typical of BALT, the lymphoid aggregates contained HEVs, sites of lymphocyte homing identified by the presence of peripheral node addressin marked by MECA-79 antibody (Figure 4E). In addition, the airway epithelium overlying BALT contained M cells, which are sites specialized for antigen entry identified by *U. europaeus* lectin binding (Figure 4F).[31,34] Lymphatics were most abundant in regions of loosely packed T cells around, but not inside, B-cell follicles of BALT (Figure 4, G–I).

Time Course of Sprouting Lymphangiogenesis in BALT

The temporal relationship between lymphocyte influx, BALT formation, and lymphangiogenesis was examined during early stages of infection. Pathogen-free lungs had few B or T cells (Supplemental Figure S3, A–C). At 3 days of infection, the number of T cells was conspicuously increased throughout the lung parenchyma. This was the earliest time point when clusters of lymphocytes, especially T cells, were found near lymphatics (Supplemental Figure S3, D–F). At 3 days, lymphatics appeared normal, but at 5 days, sprouts were present on lymphatics, and B-cell follicles were evident around airways and large vessels (Supplemental Figure S3G). T and B cells were present in the lumen of some lymphatics (Supplemental Figure S3, H and I).

Diverse Inflammatory Cells in BALT and Lung Parenchyma after Infection

Macrophages, dendritic cells, and neutrophils were abundant along T and B cells in BALT. Macrophages and dendritic cells, identified by immunoreactivity for Aif1/Iba1, were sufficiently numerous to delineate the margins of BALT (Figure 4J). Neutrophils, identified by S100A8 immunoreactivity, were scattered in BALT but were much more abundant in the airway lumen (Figure 4K). These inflammatory cells were also abundant in the lung parenchyma of infected mice (Figure 4, L and M). Lymphatics in BALT and distal branches of pulmonary veins in the lung parenchyma coursed through macrophage- and neutrophil-rich regions (Figure 4, L and M), but only the lymphatic network in BALT underwent conspicuous expansion.

Contribution of VEGFR-3 and VEGFR-2 Signaling to Lymphangiogenesis in Lung

Effect of Blocking VEGFR-3 and/or VEGFR-2 on Lung Lymphatics

To determine the contribution of VEGFR-3 and/or VEGFR-2 signaling to the expansion of the lung lymphatic network after infection, we treated mice with function-blocking antibodies to VEGFR-3 and/or VEGFR-2 from the onset of infection, and measured the abundance of lymphatics at 14 days. Lymphatics in both the lung and the trachea were

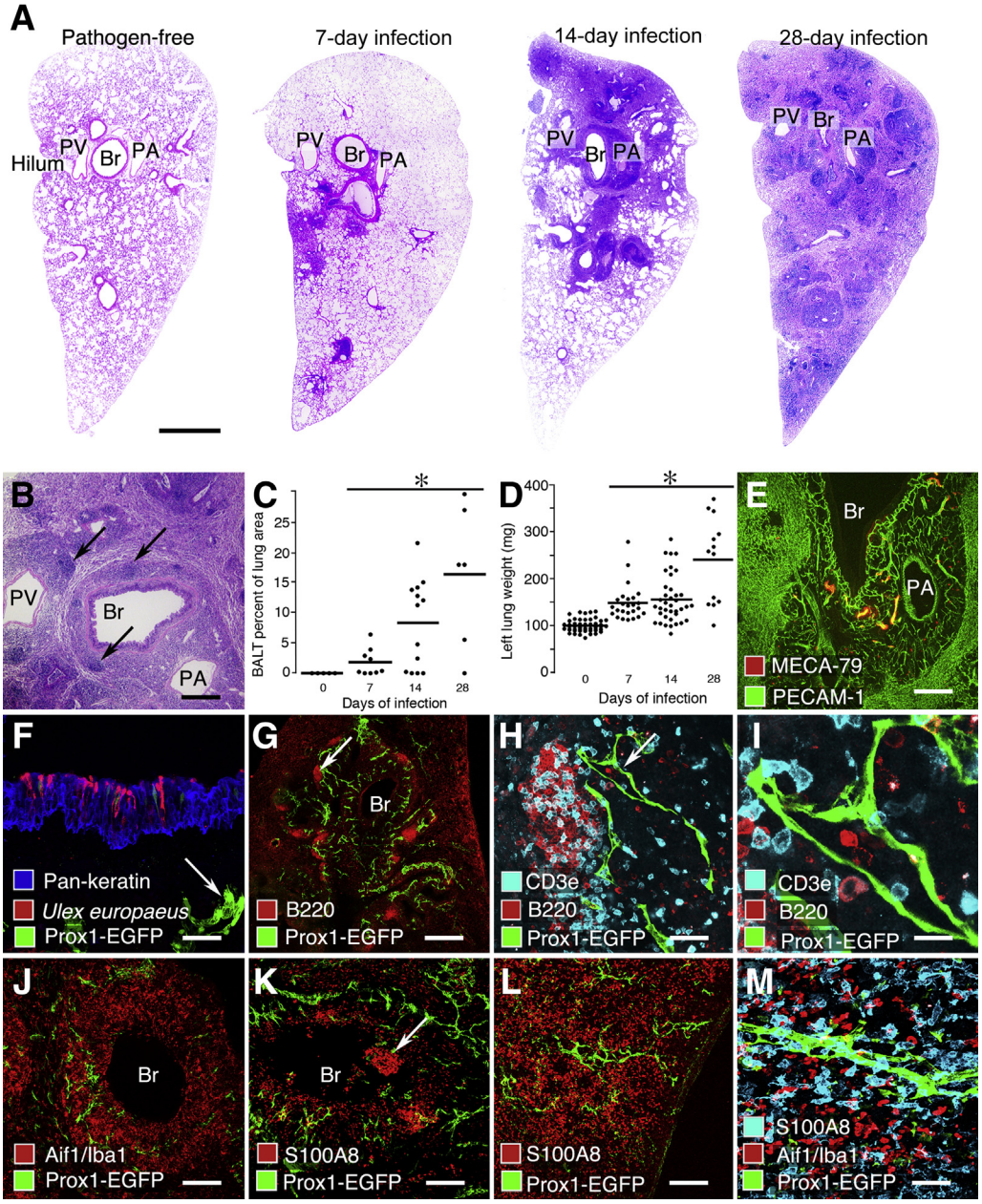

Figure 4 Lymphatics in BALT. **A:** Montage of H&E-stained sections of mouse left lung at 0, 7, 14, and 28 days after *M. pulmonis* infection. At 7 days, BALT (intense purple) is greatest in the hilum. The overall amount of BALT increases during the infection. By 28 days, the entire lung consists of regions of BALT surrounded by consolidated lung parenchyma typical of lobar pneumonia (less intense purple areas). **B:** After 28 days of infection, the main bronchus (Br) and pulmonary artery (PA) are surrounded by BALT, which has a sharp border with the lung parenchyma. The pulmonary vein (PV) has a separate cuff of BALT. Lymphoid follicles (**arrows**). **C:** Time course of increase in amount of BALT expressed as percentage of total area of H&E-stained sections of mouse left lung at 0, 7, 14, and 28 days after infection. Infected values are significantly greater than pathogen free and increase with infection duration ($*P < 0.05$; $N \geq 5$ mice per group). **D:** Time course of increase in left lung wet weight, expressed relative to the control (0 days) weight, at 0, 7, 14, and 28 days after infection. Infected values are significantly different from pathogen free; values at 28 days are different from values at 7 and 14 days ($*P < 0.05$; $N \geq 13$ mice per group). **E**—**M:** A 28-day infection. **E:** MECA-79 immunoreactivity (red) marks HEVs (**arrowheads**) in BALT around bronchus (Br) and pulmonary vein (PA). Blood vessels marked by PECAM-1 immunoreactivity (green). **F:** M cells stained by *U. europaeus* lectin (red) in the bronchial epithelium after 28 days of infection. Epithelial cells (pan-keratin, blue). Lymphatics (Prox1-EGFP, green, **arrow**). **G:** B-cell follicles (B220, red) and lymphatics (Prox1-EGFP, green) in BALT after infection for 28 days. **H:** Enlargement of B-cell follicle in **G** (**arrow**). B cells (B220, red) are more abundant than T cells (CD3e, cyan). Lymphatics (Prox1-EGFP, green, **arrow**) in the T-cell zone but not in the B-cell zone. **I:** Enlargement of perifollicular lymphatic (Prox1-EGFP, green) in **H** (**arrow**), showing B cells (B220, red) and T cells (CD3e, cyan) in the lumen. **J:** Macrophages and dendritic cells (Aif1/Iba1, red) surround lymphatics (Prox1-EGFP, green) and outline the border of BALT around a Br. **K:** Neutrophils (S100A8, red) scattered near lymphatics (Prox1-EGFP, green) in BALT around a Br and found in clumps (**arrow**) in the airway lumen. **L:** Lung parenchyma near pleura showing abundant neutrophils (S100A8, red) and scattered lymphatics (Prox1-EGFP, green). **M:** Higher magnification of region in **L** showing neutrophils (S100A8, cyan) and macrophages and dendritic cells (Aif1/Iba1, red) near lymphatics (Prox1-EGFP, green). Scale bars: 1000 μm (**A**); 400 μm (**B** and **G**); 200 μm (**E** and **J**—**L**); 50 μm (**F**, **H**, and **M**); 20 μm (**I**).

assessed to build a bridge to our previous work on lymphangiogenesis in the trachea after *M. pulmonis* infection.[17] The earlier study revealed that inhibition of VEGFR-3 alone completely inhibited lymphangiogenesis in the trachea after infection.[17] We reasoned that if a different result were obtained in the lung, the change in the trachea would enable us to bridge to the earlier findings and know whether the new experiment matched the previous one. Lymphatics were visualized in the trachea by staining for LYVE-1 but were visualized in the lung by VEGFR-3 immunoreactivity to avoid confusion by lung blood vessels with LYVE-1 immunoreactivity.

As a reference, tracheal lymphatics increased 12-fold over the pathogen-free value during infection for 14 days in mice that received control rat IgG (Supplemental Figure S4, A and B). The increase was 40% less in mice treated with the VEGFR-2−blocking antibody DC101 (Supplemental Figure S4C) and 98% less in mice treated with the VEGFR-3−blocking antibody mF4-31C1 (Supplemental Figure S4, D and F). Tracheal lymphatics in infected mice receiving the anti−VEGFR-2 and anti−VEGFR-3 antibodies together were similar to those receiving anti−VEGFR-3 alone (Supplemental Figure S4, E and F). Both resembled the lymphatics in pathogen-free controls.

The results were similar, but not identical, in the lung (Figure 5, A−F). The infected group that received control IgG had a fourfold increase in lung lymphatics over the pathogen-free baseline (Figure 5, A and B). The apparently greater increase in the trachea was more a reflection of differences in the pathogen-free baseline values in the trachea and lung than amount of increase after infection. Lung lymphatics were 68% less numerous in mice treated with VEGFR-2−blocking antibody (Figure 5C), 83% less in mice treated with VEGFR-3−blocking antibody (Figure 5D), and 99% less in mice treated with both antibodies together (Figure 5, E and F). None of the treatments had a measurable effect on the abundance of lymphatics in the lung parenchyma (Figure 5F). Values for trachea and lung in the same mice had a significant correlation by linear regression analysis, with a coefficient of determination R^2 of 0.54 ($P < 0.05$).

Effect of Blocking VEGFR-3 and/or VEGFR-2 on BALT and Lymph Nodes

The overall effect on lung inflammation of blocking VEGFR-3 and/or VEGFR-2 was assessed by examining the amount of BALT (Figure 5G) and bronchial lymph node hypertrophy. Measurements of BALT in H&E-stained sections of lungs gave similar values in all infected mice, regardless of antibody treatment (Figure 5H), and all infected groups were significantly greater than the amount in pathogen-free mice (Figure 5H). The amount of BALT in these treatment groups was similar to that found at 14 days in the earlier time course study (Figure 4C).

During the 14-day infection, bronchial lymph nodes increased sixfold in weight. Blocking VEGFR-2 and VEGFR-3 together reduced the weight by 50%, but blocking either VEGFR-2 or VEGFR-3 alone had no significant effect on lymph node weight (Figure 5I).

After having learned that blocking VEGFR-2 and/or VEGFR-3 did not change the amount of BALT, we asked if the blood vasculature of BALT was affected, to test the possibility that these inhibitors prevented angiogenesis that normally occurs as lymphoid tissue expands. Studies of BALT vasculature revealed that nonfollicular regions of BALT contained abundant blood capillaries and HEVs. The vessel types were readily distinguished because HEVs were much larger than capillaries (Figure 5J). Lymphoid follicles had fewer blood capillaries and no HEVs. When VEGFR-2 and VEGFR-3 were inhibited together throughout the 14-day infection, capillaries in BALT were less than half as numerous, but HEVs seemed unaffected (Figure 5K).

Lack of Lymphatic Sprouting after Overexpression of VEGF-A

To explore evidence for the involvement of VEGFR-2 in sprouting and growth of lung lymphatics after *M. pulmonis* infection, we asked whether VEGF-A, a potent ligand for VEGFR-2, made a contribution. To address this question, we used Clara cell secretory protein (CCSP)−VEGF-A−transgenic mice as a model in which VEGF-A expression, under the control of the CCSP promoter, triggers abundant angiogenesis in the trachea and lung when activated by doxycycline administration.[28] Sections of lungs of CCSP−VEGF-A mice taking doxycycline for 14 days had usually abundant blood vessels in the bronchial mucosa, but no expansion or sprouting of neighboring lymphatics, compared with CCSP−VEGF-A mice taking water (Supplemental Figure S4, G and H).

Persistence of Lung Lymphatics after Resolution of Infection

To build on our previous observation that newly formed lymphatics persisted in tracheas long after *M. pulmonis* infection was eliminated by antibiotic treatment,[17] we sought to determine whether the same occurred in the lung. Mice infected for 14 days were then treated for a further 14 days with vehicle or with oxytetracycline to eliminate the infection. The experiment had a clear outcome: BALT was extensive in H&E-stained sections of untreated lung, but was sparse or absent in lungs of infected mice treated with the antibiotic (Figure 6, A−D and I). However, in the same mice, the abundance of lymphatics around major bronchi and pulmonary vessels was not significantly reduced by oxytetracycline (Figure 6, E−H and J). Treatment with the antibiotic had a similar effect on bronchial lymph nodes as on BALT: lymph node weight was reduced almost to pathogen-free levels (Figure 6K).

Discussion

We sought to determine the number and distribution of lymphatics in the lung of mice, how lung lymphatics change after

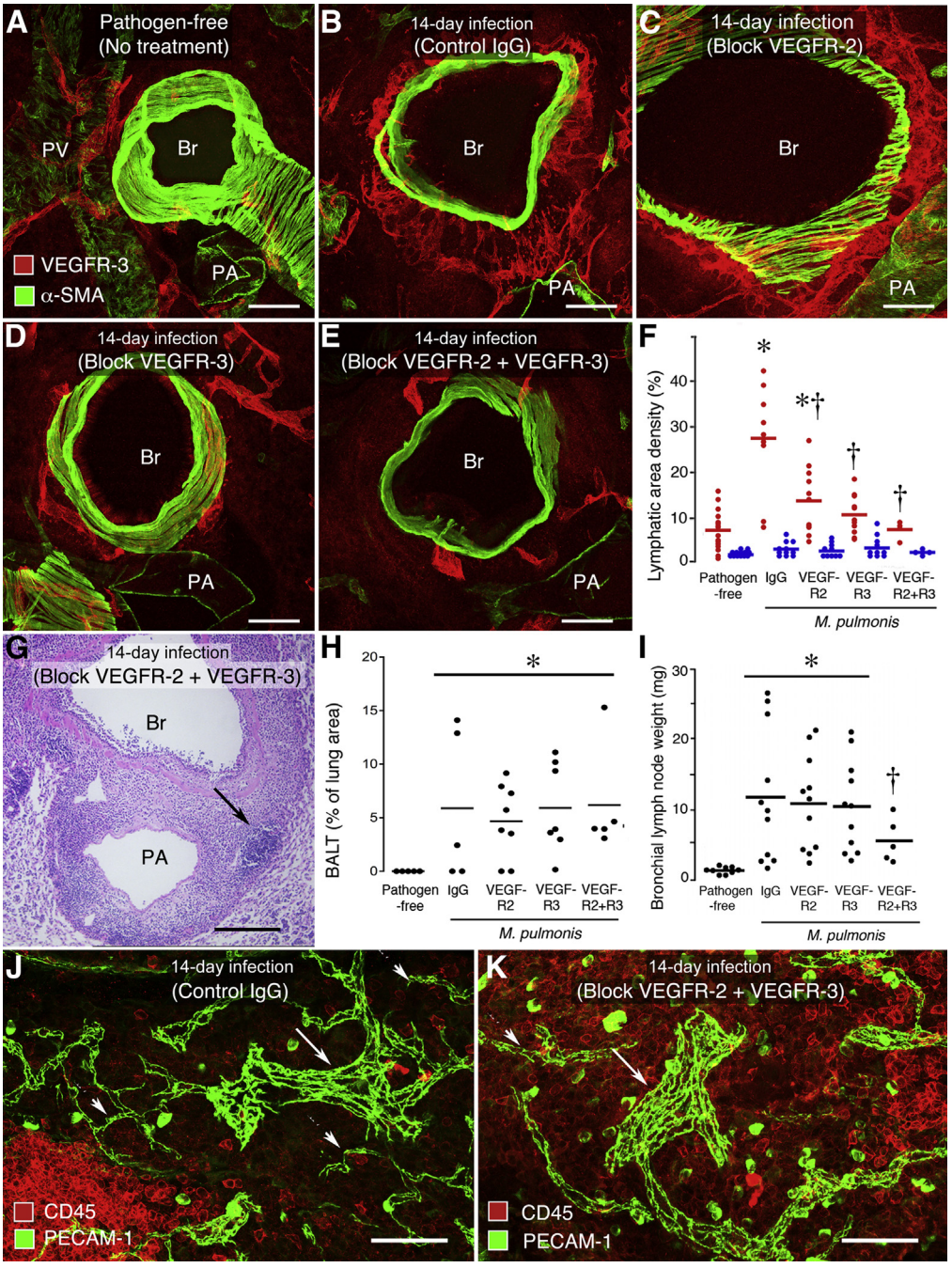

Figure 5 Effect of treatment of mice with control IgG or function-blocking antibodies to VEGFR-2 (DC101) and/or VEGFR-3 (mF4-31C1) on lymphangiogenesis and angiogenesis in lung during *M. pulmonis* infection for 14 days. Pathogen-free controls had no treatment. **A**—**E:** Lymphatics around bronchus (Br), pulmonary artery (PA), or pulmonary vein (PV) near hilum. Lung sections stained for VEGFR-3 (red) and αSMA (green). **A:** Sparse lymphatics in pathogen-free mouse. **B:** Abundant lymphatics in infected mouse treated with control IgG. **C:** Abundant lymphatics in infected mouse treated with anti—VEGFR-2. **D:** Sparse lymphatics in infected mouse treated with anti—VEGFR-3. **E:** Sparse lymphatics in infected mouse treated with anti—VEGFR-2 and anti—VEGFR-3. **F:** Relative abundance of lymphatics in lung of pathogen-free mice and infected mice treated with VEGFR blocking antibodies. Red dots represent average value for lymphatics around bronchus, pulmonary artery, and pulmonary vein in each mouse. Blue dots represent corresponding values for lung parenchyma. $^{*}P < 0.05$ compared to baseline; $^{\dagger}P < 0.05$ compared to infected mice treated with control IgG. No significant differences among lung parenchyma groups ($N = 5$ to 11 mice per group). **G:** H&E-stained section of left lung of infected mouse treated with anti—VEGFR-2 and anti—VEGFR-3 showing BALT with lymphoid follicle (**arrow**) around Br and PA. **H:** Amount of BALT, expressed as percentage of total lung area, measured in H&E-stained lung sections of pathogen-free mice and infected mice treated with VEGFR blocking antibodies. BALT was not present in lungs of pathogen-free mice. Significantly different from pathogen-free group ($^{*}P < 0.05$), but no significant difference was found among the treatment groups ($N = 5$ to 8 mice per group). **I:** Bronchial lymph node wet weight in pathogen-free mice and infected mice treated with VEGFR blocking antibodies. Significantly different from pathogen-free group ($^{*}P < 0.05$) or other groups of infected mice ($^{\dagger}P < 0.05$) ($N = 5$ to 11 mice per group). **J** and **K:** Blood vessels (PECAM-1, green) and leukocytes (CD45, red) in BALT near bronchus. Infected mouse treated with control IgG. **J:** BALT contains abundant leukocytes, blood capillaries (**arrowheads**), and HEVs (**arrow**). Infected mouse treated with anti—VEGFR-2 and anti—VEGFR-3. **K:** BALT has fewer blood capillaries (**arrowhead**), but larger blood vessels (HEVs, **arrow**) are still present.

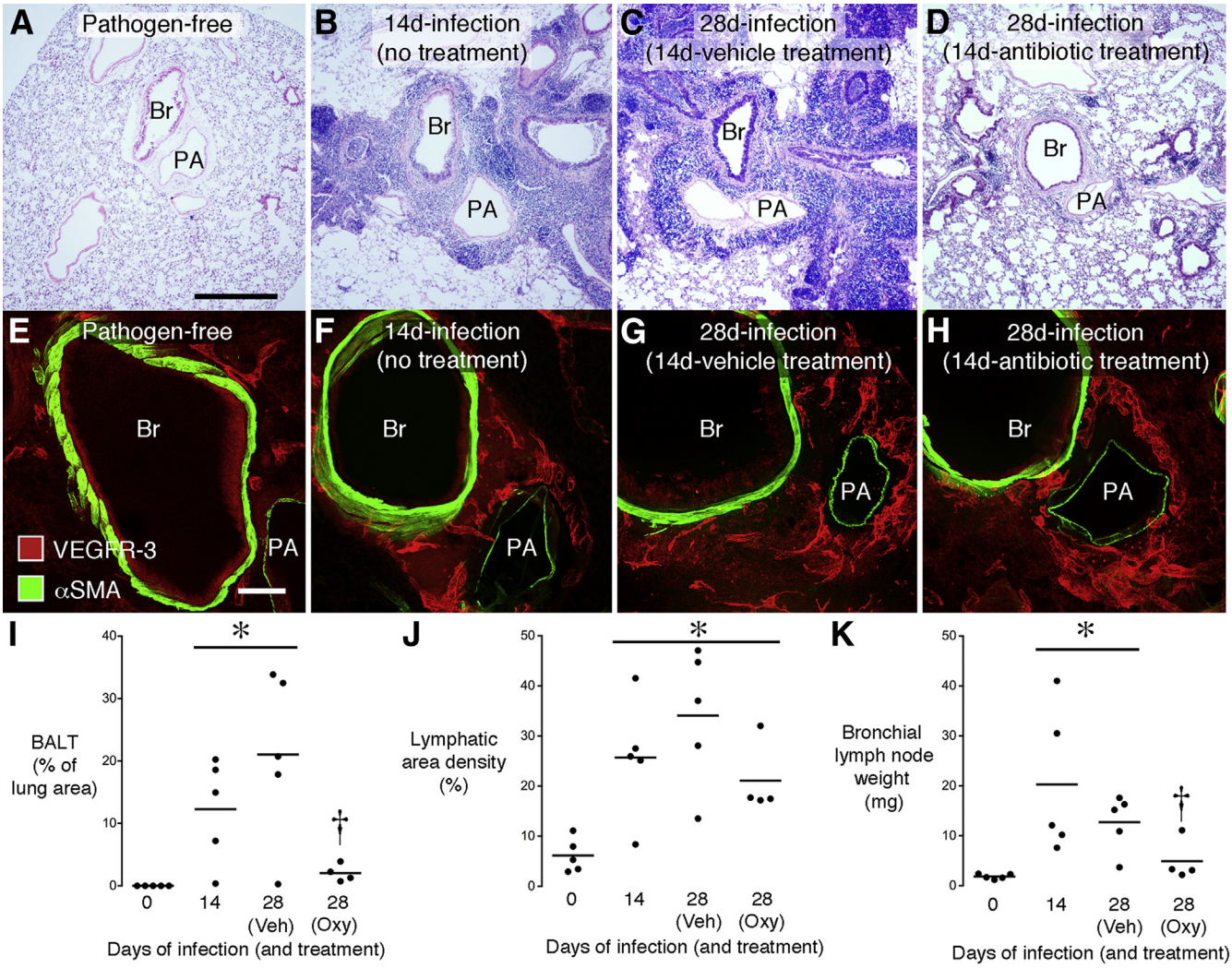

Figure 6 Reversibility of BALT formation, but not lymphangiogenesis, after *M. pulmonis* infection. H&E-stained sections of mouse left lung comparing pathogen-free state (**A**), infection for 14 days (**B**), infection for 28 days with vehicle treatment during final 14 days (**C**), and infection for 28 days with antibiotic (oxytetracycline) during final 14 days (**D**). BALT is abundant around bronchus (Br) and pulmonary artery (PA) in infected mice, except in antibiotic-treated group. Confocal microscopic images of lungs under same conditions as in **A** to **D** comparing the sparse lymphatics (VEGFR-3, red) around major Br and PA in pathogen-free lung (**E**) with the abundant lymphatics after infection, where lymphatics are similarly numerous in all infected groups (**F**–**H**). **I:** Percentage of lung sectional area occupied by BALT under same conditions as in **A** to **D**. **J:** Area density of lung lymphatics shown by VEGFR-3 immunoreactivity around major bronchi and pulmonary vessels under same conditions as in **A** to **D**. Values are greater after infection and not reduced by antibiotic (Oxy) during final 14 days of 28-day infection. **K:** Bronchial lymph node weight under same conditions as in **A** to **D**. $N = 4$ to 5 mice per group. $^{*}P < 0.05$ from pathogen-free group, $^{\dagger}P < 0.05$ from 28-day infection with vehicle (Veh) treatment.

M. pulmonis infection, the contribution of VEGFR-2 and VEGFR-3 signaling to the lymphatic growth, and the reversibility by treatment of the infection. Lungs were found to have a well-developed and regionally highly specialized lymphatic network. On infection, lymphangiogenesis was conspicuous but was restricted to regions of lymphoid tissue that formed around the major bronchi and blood vessels. Lymphatics in the distal lung parenchyma were little changed, even where inflammatory cell influx was extensive. The growth of new lymphatics in BALT was found to require signaling of both VEGFR-2 and VEGFR-3, but blocking these receptors did not prevent the formation of BALT. BALT resolved when the infection was treated with the antibiotic oxytetracycline, but not with the new lymphatics.

Relation of Murine *M. pulmonis* Infection to Human Pulmonary Disease

Mycoplasma pulmonis infection has multiple attributes for studies of sustained lung inflammation because these natural murine pathogens have co-evolved with their host to reach a balance between infection of the respiratory tract and elimination by host immune responses. Compared with transient pulmonary infections or irritants, the inflammatory stimulus provided by *M. pulmonis* is sustained and consequently leads to progressive pathological characteristics.[29] The mouse model of lymphangiogenesis in sustained lung inflammation reported herein might also be relevant to human pulmonary disease. BALT develops in several human lung diseases, including

COPD, idiopathic pulmonary fibrosis, hypersensitivity pneumonitis, and rheumatoid arthritis, where it may result from opportunistic secondary lung infections.[35,36] However, we are aware of only one clinical report that mentions the presence of lymphatics in BALT of lungs.[5] The authors of that study concluded that BALT and associated lymphatics contributed to aggravated inflammation in COPD.

Comparison of Lung Lymphatics in Pathogen-Free and Infected Mice

Most lymphatics in lungs of pathogen-free mice, as in other species, accompanied the major bronchi and blood vessels, especially pulmonary veins. Fewer lymphatics were located in the lung parenchyma. These findings are in broad agreement with a recent study of lung lymphatics in pathogen-free mice.[19] Compared with larger organisms, such as rat,[37] sheep,[38] or human,[39] a notable difference in the architecture of lymphatics in mouse lung was their almost complete absence in the visceral pleura.

From the results of previous studies of trachea in *M. pulmonis*–infected mice,[17,18,40–42] it seemed likely that lymphangiogenesis would also occur in the lung after infection, but we did not know how, when, or where it would happen. An unexpected finding in the current study was that most of the lymphangiogenesis in lungs after infection occurred in regions of BALT around the major airways and blood vessels. In this respect, our finding differed from that of a report in which no significant changes were found in lymphatics in lung inflammation induced by administration of house dust mite allergen.[19] The reason for the difference is not clear but probably involves the nature, severity, and duration of the inflammatory response under the two conditions.

Time Course of Changes in Lymphatics

In this study, much of the lymphatic growth in the lung occurred within the first 7 days after infection, but lymphangiogenesis continued for at least 28 days. The onset of lymphatic growth was more rapid in the lung than in the trachea, where lymphatic sprouting began around 7 days and was not obvious until 14 days. The slower lymphangiogenesis in the trachea could reflect the spread of infection from the lung to more proximal airways. At any rate, for this reason, we used the 14-day time point to compare the effects of VEGFR-2/VEGFR-3–blocking antibodies in lungs and trachea.

Of the markers of lymphatic phenotype examined, CCL21 was the only one that was clearly greater in infected lungs than in pathogen-free lungs. CCL21 immunoreactivity was increased not only in the newly formed lymphatics but also in the extracellular matrix. These findings are consistent with recent reports of increased CCL21 secretion by inflammatory stimuli, thereby facilitating mobilization and trafficking of dendritic cells and lymphocytes into activated lymphatics.[43–46] Increased CCL21 staining has also been reported on lung lymphatics in patients with COPD.[6]

Relationship of Changes in Lymphatics to other Inflammatory Changes

The present study showed that changes in mouse lung lymphatics after infection happened more or less in parallel with peribronchial and perivascular lymphoid cuffing by BALT and development of pneumonia. Both processes were recognized many years ago in mouse lungs after *M. pulmonis* infection,[29] but have not previously been examined in the context of lung lymphatics. Lymphangiogenesis was closely associated with the formation of BALT but not with the development of pneumonia.

Although numerous studies confirm that experimental bacterial or viral infection can induce BALT in mouse lungs,[33,47,48] lymphatics in BALT have received relatively little attention.[35] The present study showed that the peribronchial and perivascular cuffs in mouse lungs infected with *M. pulmonis* had all of the features characteristic of BALT, including the presence of HEVs,[32,49] epithelial M cells,[31,34] and B-cell follicles surrounded by T-cell zones.[30,32]

Our finding that lymphangiogenesis in the lung was largely restricted to BALT after *M. pulmonis* infection has several implications. First, it suggests that functions of the newly formed lymphatics relate more to BALT than to general fluid balance or cell trafficking in other regions of the lung. For immune cells that enter the lung via HEVs in BALT, the newly formed lymphatics are likely to be an exit route.[11] In this context, the location of lymphatics in peripheral regions of BALT some distance from the airway epithelium indicates that antigens and antigen-presenting cells traverse the thickness of BALT to reach lymphatics. Our observation of leukocytes in the lumen of lymphatics in BALT suggests that the newly formed lymphatics could be functional in terms of immune cell trafficking. The finding of VEGF-C and lymphangiogenesis in BALT suggests that local factors drive lymphatic growth. B cells have been claimed to drive lymphangiogenesis in inflamed lymph nodes.[25] In the present study, VEGF-C–containing cells and the newly formed lymphatics were located in T-cell regions of BALT, but not in B-cell follicles. The involvement of T or B cells is suggested by evidence that lymphangiogenesis does not occur after *M. pulmonis* infection in immunodeficient recombination-activating gene–deficient mice or B-cell–deficient mice.[40]

There is no consensus on whether BALT is beneficial or detrimental to the host after *M. pulmonis* infection. Like other features of sustained inflammation, BALT is probably both good and bad for different aspects of disease. Because BALT changes normal lung structure and could affect gas exchange, it would appear to be bad for the lung. However, because BALT could help confine the disease to the airways and lungs and prevent dissemination to distant sites, it would be beneficial for the host overall. In recombination-activating gene mice, severe combined immunodeficient mice, B-cell–deficient mice, and mice treated with the immunosuppressant cyclophosphamide, BALT does not

develop after *M. pulmonis* infection and the lungs are relatively normal. However, the bacteria disseminate throughout the body and infect the pericardium, liver, spleen, and even joints, where severe arthritis can develop.[40,50–52]

Dependency of Lung Lymphatic Growth on VEGFR-3 and VEGFR-2 Signaling

Our studies with blocking antibodies showed that VEGFR-3 signaling was the main, but not the only, driving force for lymphangiogenesis in lungs after *M. pulmonis* infection. The finding that VEGFR-3 signaling is dominant is consistent with the presence of VEGF-C in inflammatory cells in BALT and with evidence for lymphatic growth in other organs.[20] However, VEGFR-2 signaling also had a role in the lung. The involvement of both VEGFR-3 and VEGFR-2 in lymphangiogenesis has been shown in skin,[23,53–55] lymph nodes,[25,56] cornea,[57] and tumors.[26] In all locations, VEGFR-3 has the stronger effect. VEGF-A is reported to drive lymphatic growth through VEGFR-2 in embryonic mouse lungs,[58] but, to our knowledge, this has not been examined in adult lungs. The present studies of VEGF-A overexpression in CC10–VEGF-A mice detected no lymphangiogenesis, despite the robust angiogenesis. The relative lack of changes in lymphatics in distal regions of lung parenchyma, despite the presence of abundant inflammatory cells, indicates that the microenvironmental conditions necessary for lymphangiogenesis differ in BALT from other regions of the lung.

How VEGFR-2 signaling contributes to lymphangiogenesis is not well understood. Several direct and indirect mechanisms have been proposed. Because both VEGFR-3 and VEGFR-2 are expressed on lymphatic endothelial cells,[20] it has been proposed that VEGF-A and VEGF-C stimulate their respective receptors to promote different aspects of lymphangiogenesis, radial enlargement, and lymphatic sprouting.[55] VEGF-A, and even more potently VEGF-C, can promote the formation of VEGFR-2/VEGFR-3 heterodimers that can be activated by either growth factor.[59] Antibodies that prevent VEGFR-3/VEGFR-2 heterodimer formation can inhibit both angiogenesis and lymphangiogenesis.[60] Signaling through heterodimers can also be influenced by regulatory molecules, such as Bmx kinase, that modulate downstream signaling pathways.[61]

VEGF-A can recruit macrophages, promote angiogenesis, and induce plasma extravasation. Because some macrophages secrete VEGF-C, inhibiting VEGFR-2 signaling could reduce lymphangiogenesis by suppressing macrophage influx.[20,57] Inhibition of VEGFR-2 signaling could also inhibit lymphangiogenesis by reducing plasma leakage and thereby reduce mediators from extravasated plasma that contribute to macrophage or immune cell recruitment, activation of extracellular proteases, or other processes that produce lymphangiogenic factors.

Issues Still to be Resolved about Lung Lymphatics

Further studies will be needed to address the complexities of VEGFR-3/VEGFR-2 interactions in lymphangiogenesis. Experiments using CCSP–VEGF-A–transgenic mice showed that VEGF-A overexpression in respiratory tract epithelial cells produced angiogenesis without lymphangiogenesis in the lungs. These results are consistent with earlier findings in the trachea,[28] but could appear inconsistent with evidence of the involvement of VEGFR-2 signaling in the growth of lymphatics in the lung after *M. pulmonis* infection. A possible explanation could be that the human VEGF-A (VEGF165), and not mouse VEGF-A (VEGF164), is overexpressed in this transgenic mouse[62] and could influence the ability to promote VEGFR-3/VEGFR-2 heterodimer formation and downstream signaling in the host mouse.

Among the other issues requiring further work is the identity of cells that produce VEGF-C and/or VEGF-D in inflamed tissues. Additional work is also needed to determine the functionality of new lymphatics that grow in the lung in sustained inflammation. Although many technical challenges need to be overcome, there is hope that live-imaging technologies will provide insights into their function.[12,46,63,64]

Although BALT was required for the growth of new lymphatic vessels, the converse appears not to be true. Prevention of lymphangiogenesis by treatment with antibodies that blocked both VEGFR-3 and VEGFR-2 did not prevent BALT development. However, in agreement with previous studies of inflamed skin,[25] the antibody combination did reduce the enlargement of the draining lymph node that occurs in *M. pulmonis* infection. The mechanism of suppression of lymph node growth is not known, but could involve the reduced cell trafficking and fluid drainage from the inflamed organ to the lymph node and reduced angiogenesis and lymphangiogenesis in the lymph node.

The finding of lymphangiogenesis occurring mainly within BALT in infected lungs resembles features of Hashimoto's thyroiditis in humans and in transgenic mouse models[65,66] and human renal transplant rejection.[67,68] Sustained immune cell activity and defective lymphatic drainage are thought to trigger the formation of ectopic germinal centers and lymphangiogenesis in such chronic inflammatory conditions.[69] New patterns of lymph flow are established that result in a self-perpetuating feedback loop that sustains the local immune response. In this way, lymphoid cells and lymphatics are mutually interdependent. Persistence of new lung lymphatics after the infection resolves could accelerate or amplify responses to subsequent infections.

Summary

In this study, we sought to learn how lung lymphatics change in sustained inflammation and to understand the mechanism of the changes. After *M. pulmonis* infection in C57BL/6 mice, BALT formed around major bronchi and pulmonary blood vessels. As BALT accumulated, lymphatics grew by sprouting

lymphangiogenesis preferentially within T-cell regions that contained VEGF-C–producing CD45-positive cells. The new lymphatics had higher than normal expression of CCL21. Little lymphatic growth occurred in distal regions of lung parenchyma, despite the presence of abundant inflammatory cells in regions of pneumonia. Experiments using function-blocking antibodies revealed that signaling through the two VEGF-C–driven receptors, VEGFR-3 and VEGFR-2, accounted for 99% of the lymphangiogenesis in the lung under these conditions. The new lymphatics were remarkably persistent after resolution of the infection by treatment with the antibiotic oxytetracycline. The lack of regression of the new lung lymphatics, despite regression of the BALT in which they grew, could exaggerate responses to subsequent infections.

Acknowledgments

We thank Bronek Pytowski (ImClone Incorporated, New York, NY) for providing the blocking antibodies to mouse VEGFR-2 and VEGFR-3, Caitlin Sorensen and Oishee Bose [University of California, San Francisco (UCSF), San Francisco, CA] for help in preparing stocks of *M. pulmonis*, Jennifer Bolen (UCSF) for H&E staining, and members of the McDonald laboratory for many helpful comments and suggestions.

Supplemental Data

Supplemental material for this article can be found at *http://dx.doi.org/10.1016/j.ajpath.2014.01.021*.

References

1. El-Chemaly S, Levine SJ, Moss J: Lymphatics in lung disease. Ann N Y Acad Sci 2008, 1131:195–202
2. Schraufnagel DE: Lung lymphatic anatomy and correlates. Pathophysiology 2010, 17:337–343
3. Ebina M: Remodeling of airway walls in fatal asthmatics decreases lymphatic distribution: beyond thickening of airway smooth muscle layers. Allergol Int 2008, 57:165–174
4. Mandal RV, Mark EJ, Kradin RL: Organizing pneumonia and pulmonary lymphatic architecture in diffuse alveolar damage. Hum Pathol 2008, 39:1234–1238
5. Mori M, Andersson CK, Svedberg KA, Glader P, Bergqvist A, Shikhagaie M, Lofdahl CG, Erjefalt JS: Appearance of remodelled and dendritic cell-rich alveolar-lymphoid interfaces provides a structural basis for increased alveolar antigen uptake in chronic obstructive pulmonary disease. Thorax 2013, 68:521–531
6. Mori M, Andersson CK, Graham GJ, Lofdahl CG, Erjefalt JS: Increased number and altered phenotype of lymphatic vessels in peripheral lung compartments of patients with COPD. Respir Res 2013, 14:65
7. El-Chemaly S, Malide D, Zudaire E, Ikeda Y, Weinberg BA, Pacheco-Rodriguez G, Rosas IO, Aparicio M, Ren P, MacDonald SD, Wu HP, Nathan SD, Cuttitta F, McCoy JP, Gochuico BR, Moss J: Abnormal lymphangiogenesis in idiopathic pulmonary fibrosis with insights into cellular and molecular mechanisms. Proc Natl Acad Sci U S A 2009, 106:3958–3963
8. Yamashita M, Iwama N, Date F, Chiba R, Ebina M, Miki H, Yamauchi K, Sawai T, Nose M, Sato S, Takahashi T, Ono M: Characterization of lymphangiogenesis in various stages of idiopathic diffuse alveolar damage. Hum Pathol 2009, 40:542–551
9. Ebina M, Shibata N, Ohta H, Hisata S, Tamada T, Ono M, Okaya K, Kondo T, Nukiwa T: The disappearance of subpleural and interlobular lymphatics in idiopathic pulmonary fibrosis. Lymphat Res Biol 2010, 8:199–207
10. Leak LV: Lymphatic removal of fluids and particles in the mammalian lung. Environ Health Perspect 1980, 35:55–76
11. Randolph GJ, Angeli V, Swartz MA: Dendritic-cell trafficking to lymph nodes through lymphatic vessels. Nat Rev Immunol 2005, 5:617–628
12. Thornton EE, Looney MR, Bose O, Sen D, Sheppard D, Locksley R, Huang X, Krummel MF: Spatiotemporally separated antigen uptake by alveolar dendritic cells and airway presentation to T cells in the lung. J Exp Med 2012, 209:1183–1199
13. Kunstfeld R, Hirakawa S, Hong YK, Schacht V, Lange-Asschenfeldt B, Velasco P, Lin C, Fiebiger E, Wei X, Wu Y, Hicklin D, Bohlen P, Detmar M: Induction of cutaneous delayed-type hypersensitivity reactions in VEGF-A transgenic mice results in chronic skin inflammation associated with persistent lymphatic hyperplasia. Blood 2004, 104:1048–1057
14. Zhang Q, Lu Y, Proulx ST, Guo R, Yao Z, Schwarz EM, Boyce BF, Xing L: Increased lymphangiogenesis in joints of mice with inflammatory arthritis. Arthritis Res Ther 2007, 9:R118
15. Alexander JS, Chaitanya GV, Grisham MB, Boktor M: Emerging roles of lymphatics in inflammatory bowel disease. Ann N Y Acad Sci 2010, 1207(Suppl 1):E75–E85
16. Huggenberger R, Ullmann S, Proulx ST, Pytowski B, Alitalo K, Detmar M: Stimulation of lymphangiogenesis via VEGFR-3 inhibits chronic skin inflammation. J Exp Med 2010, 207:2255–2269
17. Baluk P, Tammela T, Ator E, Lyubynska N, Achen MG, Hicklin DJ, Jeltsch M, Petrova TV, Pytowski B, Stacker SA, Yla-Herttuala S, Jackson DG, Alitalo K, McDonald DM: Pathogenesis of persistent lymphatic vessel hyperplasia in chronic airway inflammation. J Clin Invest 2005, 115:247–257
18. Yao LC, Baluk P, Feng J, McDonald DM: Steroid-resistant lymphatic remodeling in chronically inflamed mouse airways. Am J Pathol 2010, 176:1525–1541
19. Kretschmer S, Dethlefsen I, Hagner-Benes S, Marsh LM, Garn H, Konig P: Visualization of intrapulmonary lymph vessels in healthy and inflamed murine lung using CD90/Thy-1 as a marker. PLoS One 2013, 8:e55201
20. Tammela T, Alitalo K: Lymphangiogenesis: molecular mechanisms and future promise. Cell 2010, 140:460–476
21. Pytowski B, Goldman J, Persaud K, Wu Y, Witte L, Hicklin DJ, Skobe M, Boardman KC, Swartz MA: Complete and specific inhibition of adult lymphatic regeneration by a novel VEGFR-3 neutralizing antibody. J Natl Cancer Inst 2005, 97:14–21
22. Bock F, Onderka J, Dietrich T, Bachmann B, Pytowski B, Cursiefen C: Blockade of VEGFR3-signalling specifically inhibits lymphangiogenesis in inflammatory corneal neovascularisation. Graefes Arch Clin Exp Ophthalmol 2008, 246:115–119
23. Goldman J, Rutkowski JM, Shields JD, Pasquier MC, Cui Y, Schmokel HG, Willey S, Hicklin DJ, Pytowski B, Swartz MA: Cooperative and redundant roles of VEGFR-2 and VEGFR-3 signaling in adult lymphangiogenesis. FASEB J 2007, 21:1003–1012
24. Guo R, Zhou Q, Proulx ST, Wood R, Ji RC, Ritchlin CT, Pytowski B, Zhu Z, Wang YJ, Schwarz EM, Xing L: Inhibition of lymphangiogenesis and lymphatic drainage via vascular endothelial growth factor receptor 3 blockade increases the severity of inflammation in a mouse model of chronic inflammatory arthritis. Arthritis Rheum 2009, 60:2666–2676
25. Angeli V, Ginhoux F, Llodra J, Quemeneur L, Frenette PS, Skobe M, Jessberger R, Merad M, Randolph GJ: B cell-driven lymphangiogenesis in inflamed lymph nodes enhances dendritic cell mobilization. Immunity 2006, 24:203–215
26. Roberts N, Kloos B, Cassella M, Podgrabinska S, Persaud K, Wu Y, Pytowski B, Skobe M: Inhibition of VEGFR-3 activation with the antagonistic antibody more potently suppresses lymph node and distant metastases than inactivation of VEGFR-2. Cancer Res 2006, 66:2650–2657

27. Choi I, Chung HK, Ramu S, Lee HN, Kim KE, Lee S, Yoo J, Choi D, Lee YS, Aguilar B, Hong YK: Visualization of lymphatic vessels by Prox1-promoter directed GFP reporter in a bacterial artificial chromosome-based transgenic mouse. Blood 2011, 117: 362−365
28. Baluk P, Lee CG, Link H, Ator E, Haskell A, Elias JA, McDonald DM: Regulated angiogenesis and vascular regression in mice overexpressing vascular endothelial growth factor in airways. Am J Pathol 2004, 165:1071−1085
29. Lindsey JR, Cassell H: Experimental Mycoplasma pulmonis infection in pathogen-free mice: models for studying mycoplasmosis of the respiratory tract. Am J Pathol 1973, 72:63−90
30. Bienenstock J, McDermott MR: Bronchus- and nasal-associated lymphoid tissues. Immunol Rev 2005, 206:22−31
31. Pabst R, Tschernig T: Bronchus-associated lymphoid tissue: an entry site for antigens for successful mucosal vaccinations? Am J Respir Cell Mol Biol 2010, 43:137−141
32. Randall TD: Bronchus-associated lymphoid tissue (BALT) structure and function. Adv Immunol 2010, 107:187−241
33. Randall TD, Carragher DM, Rangel-Moreno J: Development of secondary lymphoid organs. Annu Rev Immunol 2008, 26:627−650
34. Tango M, Suzuki E, Gejyo F, Ushiki T: The presence of specialized epithelial cells on the bronchus-associated lymphoid tissue (BALT) in the mouse. Arch Histol Cytol 2000, 63:81−89
35. Carragher DM, Rangel-Moreno J, Randall TD: Ectopic lymphoid tissues and local immunity. Semin Immunol 2008, 20:26−42
36. Rangel-Moreno J, Hartson L, Navarro C, Gaxiola M, Selman M, Randall TD: Inducible bronchus-associated lymphoid tissue (iBALT) in patients with pulmonary complications of rheumatoid arthritis. J Clin Invest 2006, 116:3183−3194
37. Ohtani O, Ohtani Y: Organization and developmental aspects of lymphatic vessels. Arch Histol Cytol 2008, 71:1−22
38. Albertine KH, Wiener-Kronish JP, Roos PJ, Staub NC: Structure, blood supply, and lymphatic vessels of the sheep's visceral pleura. Am J Anat 1982, 165:277−294
39. Miller W: The Lung. Springfield, IL, Charles C. Thomas, 1937, pp 209
40. Aurora AB, Baluk P, Zhang D, Sidhu SS, Dolganov GM, Basbaum C, McDonald DM, Killeen N: Immune complex-dependent remodeling of the airway vasculature in response to a chronic bacterial infection. J Immunol 2005, 175:6319−6326
41. Baluk P, Fuxe J, Hashizume H, Romano T, Lashnits E, Butz S, Vestweber D, Corada M, Molendini C, Dejana E, McDonald DM: Functionally specialized junctions between endothelial cells of lymphatic vessels. J Exp Med 2007, 204:2349−2362
42. Baluk P, Yao LC, Feng J, Romano T, Jung SS, Schreiter JL, Yan L, Shealy DJ, McDonald DM: TNF-alpha drives remodeling of blood vessels and lymphatics in sustained airway inflammation in mice. J Clin Invest 2009, 119:2954−2964
43. Johnson LA, Jackson DG: Inflammation-induced secretion of CCL21 in lymphatic endothelium is a key regulator of integrin-mediated dendritic cell transmigration. Int Immunol 2010, 22:839−849
44. Tal O, Lim HY, Gurevich I, Milo I, Shipony Z, Ng LG, Angeli V, Shakhar G: DC mobilization from the skin requires docking to immobilized CCL21 on lymphatic endothelium and intralymphatic crawling. J Exp Med 2011, 208:2141−2153
45. Vigl B, Aebischer D, Nitschke M, Iolyeva M, Rothlin T, Antsiferova O, Halin C: Tissue inflammation modulates gene expression of lymphatic endothelial cells and dendritic cell migration in a stimulus-dependent manner. Blood 2011, 118:205−215
46. Weber M, Hauschild R, Schwarz J, Moussion C, de Vries I, Legler DF, Luther SA, Bollenbach T, Sixt M: Interstitial dendritic cell guidance by haptotactic chemokine gradients. Science 2013, 339: 328−332
47. Moyron-Quiroz JE, Rangel-Moreno J, Kusser K, Hartson L, Sprague F, Goodrich S, Woodland DL, Lund FE, Randall TD: Role of inducible bronchus associated lymphoid tissue (iBALT) in respiratory immunity. Nat Med 2004, 10:927−934
48. Foo SY, Phipps S: Regulation of inducible BALT formation and contribution to immunity and pathology. Mucosal Immunol 2010, 3:537−544
49. Rosen SD: Ligands for L-selectin: homing, inflammation, and beyond. Annu Rev Immunol 2004, 22:129−156
50. Singer SH, Ford M, Kirschstein RL: Respiratory diseases in cyclophosphamide-treated mice, I: increased virulence of Mycoplasma pulmonis. Infect Immun 1972, 5:953−956
51. Evengard B, Sandstedt K, Bolske G, Feinstein R, Riesenfelt-Orn I, Smith CI: Intranasal inoculation of Mycoplasma pulmonis in mice with severe combined immunodeficiency (SCID) causes a wasting disease with grave arthritis. Clin Exp Immunol 1994, 98:388−394
52. Cartner SC, Lindsey JR, Gibbs-Erwin J, Cassell GH, Simecka JW: Roles of innate and adaptive immunity in respiratory mycoplasmosis. Infect Immun 1998, 66:3485−3491
53. Nagy JA, Vasile E, Feng D, Sundberg C, Brown LF, Detmar MJ, Lawitts JA, Benjamin L, Tan X, Manseau EJ, Dvorak AM, Dvorak HF: Vascular permeability factor/vascular endothelial growth factor induces lymphangiogenesis as well as angiogenesis. J Exp Med 2002, 196:1497−1506
54. Hong YK, Lange-Asschenfeldt B, Velasco P, Hirakawa S, Kunstfeld R, Brown LF, Bohlen P, Senger DR, Detmar M: VEGF-A promotes tissue repair-associated lymphatic vessel formation via VEGFR-2 and the alpha1beta1 and alpha2beta1 integrins. FASEB J 2004, 18:1111−1113
55. Wirzenius M, Tammela T, Uutela M, He Y, Odorisio T, Zambruno G, Nagy JA, Dvorak HF, Yla-Herttuala S, Shibuya M, Alitalo K: Distinct vascular endothelial growth factor signals for lymphatic vessel enlargement and sprouting. J Exp Med 2007, 204:1431−1440
56. Halin C, Tobler NE, Vigl B, Brown LF, Detmar M: VEGF-A produced by chronically inflamed tissue induces lymphangiogenesis in draining lymph nodes. Blood 2007, 110:3158−3167
57. Cursiefen C, Chen L, Borges LP, Jackson D, Cao J, Radziejewski C, D'Amore PA, Dana MR, Wiegand SJ, Streilein JW: VEGF-A stimulates lymphangiogenesis and hemangiogenesis in inflammatory neovascularization via macrophage recruitment. J Clin Invest 2004, 113:1040−1050
58. Mallory BP, Mead TJ, Wiginton DA, Kulkarni RM, Greenberg JM, Akeson AL: Lymphangiogenesis in the developing lung promoted by VEGF-A. Microvasc Res 2006, 72:62−73
59. Nilsson I, Bahram F, Li X, Gualandi L, Koch S, Jarvius M, Soderberg O, Anisimov A, Kholova I, Pytowski B, Baldwin M, Yla-Herttuala S, Alitalo K, Kreuger J, Claesson-Welsh L: VEGF receptor 2/-3 heterodimers detected in situ by proximity ligation on angiogenic sprouts. EMBO J 2010, 29:1377−1388
60. Tvorogov D, Anisimov A, Zheng W, Leppanen VM, Tammela T, Laurinavicius S, Holnthoner W, Helotera H, Holopainen T, Jeltsch M, Kalkkinen N, Lankinen H, Ojala PM, Alitalo K: Effective suppression of vascular network formation by combination of antibodies blocking VEGFR ligand binding and receptor dimerization. Cancer Cell 2010, 18:630−640
61. Jones D, Xu Z, Zhang H, He Y, Kluger MS, Chen H, Min W: Functional analyses of the bone marrow kinase in the X chromosome in vascular endothelial growth factor-induced lymphangiogenesis. Arterioscler Thromb Vasc Biol 2010, 30:2553−2561
62. Lee CG, Link H, Baluk P, Homer RJ, Chapoval S, Bhandari V, Kang MJ, Cohn L, Kim YK, McDonald DM, Elias JA: Vascular endothelial growth factor (VEGF) induces remodeling and enhances TH2-mediated sensitization and inflammation in the lung. Nat Med 2004, 10:1095−1103
63. Looney MR, Thornton EE, Sen D, Lamm WJ, Glenny RW, Krummel MF: Stabilized imaging of immune surveillance in the mouse lung. Nat Methods 2011, 8:91−96
64. Proulx ST, Luciani P, Alitalo A, Mumprecht V, Christiansen AJ, Huggenberger R, Leroux JC, Detmar M: Non-invasive dynamic near-infrared imaging and quantification of vascular leakage in vivo. Angiogenesis 2013, 16:525−540

65. Furtado GC, Marinkovic T, Martin AP, Garin A, Hoch B, Hubner W, Chen BK, Genden E, Skobe M, Lira SA: Lymphotoxin beta receptor signaling is required for inflammatory lymphangiogenesis in the thyroid. Proc Natl Acad Sci U S A 2007, 104:5026–5031
66. Marinkovic T, Garin A, Yokota Y, Fu YX, Ruddle NH, Furtado GC, Lira SA: Interaction of mature CD3+CD4+ T cells with dendritic cells triggers the development of tertiary lymphoid structures in the thyroid. J Clin Invest 2006, 116:2622–2632
67. Kerjaschki D, Huttary N, Raab I, Regele H, Bojarski-Nagy K, Bartel G, Krober SM, Greinix H, Rosenmaier A, Karlhofer F, Wick N, Mazal PR: Lymphatic endothelial progenitor cells contribute to de novo lymphangiogenesis in human renal transplants. Nat Med 2006, 12:230–234
68. Kerjaschki D, Regele HM, Moosberger I, Nagy-Bojarski K, Watschinger B, Soleiman A, Birner P, Krieger S, Hovorka A, Silberhumer G, Laakkonen P, Petrova T, Langer B, Raab I: Lymphatic neoangiogenesis in human kidney transplants is associated with immunologically active lymphocytic infiltrates. J Am Soc Nephrol 2004, 15:603–612
69. Thaunat O, Kerjaschki D, Nicoletti A: Is defective lymphatic drainage a trigger for lymphoid neogenesis? Trends Immunol 2006, 27:441–445